Structural characterization of nanostructures grown by Ni metal induced lateral crystallization of amorphous-Si

G. Z. Radnóczi, E. Dodony, G. Battistig, N. Vouroutzis, P. Kavouras, J. Stoemenos, N. Frangis, A. Kovács, and B. Pécz

Citation: Journal of Applied Physics **119**, 065303 (2016); doi: 10.1063/1.4941349
View online: http://dx.doi.org/10.1063/1.4941349
View Table of Contents: http://scitation.aip.org/content/aip/journal/jap/119/6?ver=pdfcov
Published by the AIP Publishing

Structural characterization of nanostructures grown by Ni metal induced lateral crystallization of amorphous-Si

G. Z. Radnóczi,[1] E. Dodony,[1,2] G. Battistig,[1] N. Vouroutzis,[3] P. Kavouras,[3] J. Stoemenos,[3] N. Frangis,[3] A. Kovács,[4] and B. Pécz[1,a)]
[1]*Institute for Technical Physics and Materials Science, Centre for Energy Research, Hungarian Academy of Sciences, MTA EK MFA, 1121 Budapest, Konkoly-Thege M. u. 29-33, Hungary*
[2]*Doctoral School of Physics at Eötvös Loránd University, 1117, Budapest, Pázmány Péter sétány 1/a, Hungary*
[3]*Department of Physics, Aristotle University of Thessaloniki, GR-54124 Thessaloniki, Greece*
[4]*Ernst Ruska-Centre for Microscopy and Spectroscopy with Electrons, Peter Grünberg Institute, Forschungszentrum Jülich, Jülich D-52425, Germany*

(Received 2 October 2015; accepted 23 January 2016; published online 9 February 2016)

The nickel metal induced lateral crystallization of amorphous silicon is studied by transmission electron microscopy in the range of temperatures from 413 to 521 °C. The structural characteristics of the whiskers grown at 413 °C are compared to the grains grown at 600 °C, where both Metal Induced Lateral Crystallization (MILC) and Solid Phase Crystallization (SPC) are involved. At 413 °C, long whiskers are formed at any crystallographic direction almost free of defects. In contrary, whiskers grown by MILC around 600 °C are crystallized along the ⟨111⟩ directions. These differences are attributed to the low crystallization rate and suppression of the SPC process. The activation energy of the pure MILC was measured in the order of 2 eV. The effect of Ni on the crystallization rate is studied by *in-situ* heating experiments inside the microscope. The role of contamination that can inhibit MILC is discussed. The cases of MILC process under limited Ni and unlimited Ni source were studied and compared to *in-situ* annealing experiments. The crystallization rate is strongly influenced by the neighbouring Ni sources; this long-range interaction is attributed to the requirement of a critical Ni concentration in amorphous silicon before the initiation of the MILC process. The long-range interaction can enhance crystallization along a certain direction. The transition from MILC to SPC and the change of the crystallization mode due to the lack of Ni are discussed. The beneficial effect of long annealing at 413 °C is also discussed.
 [http://dx.doi.org/10.1063/1.4941349]

I. INTRODUCTION

The crystallization of amorphous silicon (a-Si) thin films below 600 °C is essential for device processing on inexpensive substrates, like soft glass, for the production of Thin Film Transistor (TFT), in order to drive Liquid Crystal Display (LCD), organic light-emitting diodes with poly-Si TFTs, solar cells, and sensors.[1–3] For lowering the crystallization temperature of a-Si, several methods have been used, such as solid-phase crystallization (SPC),[4] Rapid Thermal Annealing (RTA),[5] and Excimer Laser Annealing (ELA).[6] The SPC method has the advantage of low cost; however, it is hampered by the need for elevated temperatures above 600 °C and also long processing time. The RTA method is essentially a high-temperature process, and many substrates, including most forms of glasses, cannot withstand this process. Although ELA gives large, high quality crystallites, it is an expensive technique and requires complex facilities; moreover, it also has the drawback of poor uniformity. Metal Induced Crystallization (MIC) is a process in which an amorphous semiconductor undergoes a transformation to a crystalline state at a low temperature under the presence of a metal, such as aluminium, nickel, gold, silver, etc.[7] A specific version of MIC, namely, Metal Induced Lateral Crystallization (MILC) process, has been introduced, by which the a-Si thin film can be crystallized laterally at a temperature below 500 °C; in this case, no laser annealing is required, and high-performance TFTs have been fabricated on these films.[8] Therefore, MILC has been proposed as an alternative low temperature mechanism for crystallization of a-Si films. Among the metals employed for the study of the MILC, the preferred metal up till date has been nickel (Ni) due to its low residual metal contamination in the poly-Si region.[9] The Ni-metal induced lateral crystallization (Ni-MILC) is an extension of the MIC process; it is based on the formation of nickel di-silicide ($NiSi_2$) precipitates and their one-dimensional migration. For the Ni-MILC process, at first, thin Ni pads are formed by lithography on the a-Si film, which are then annealed at 250 °C for 10 min. The Ni reacts with the Si in the pads forming polycrystalline $NiSi_2$ there (see details in Section II). Crystallization of the a-Si starts around the pads even at 413 °C, with the $NiSi_2$ grains acting as seeds, as shown in Fig. 1. In this way, long, needle-like Si grains (whiskers) are formed.[10]

A. The standard Ni-MILC process

The Ni-MILC growth mechanism at first proposed by Hayzelden and Batstone[10] also by Jang *et al.*[11] and Cheng *et al.*[12] can be described as follows. The $NiSi_2$ precipitates

a)pecz@mfa.kfki.hu

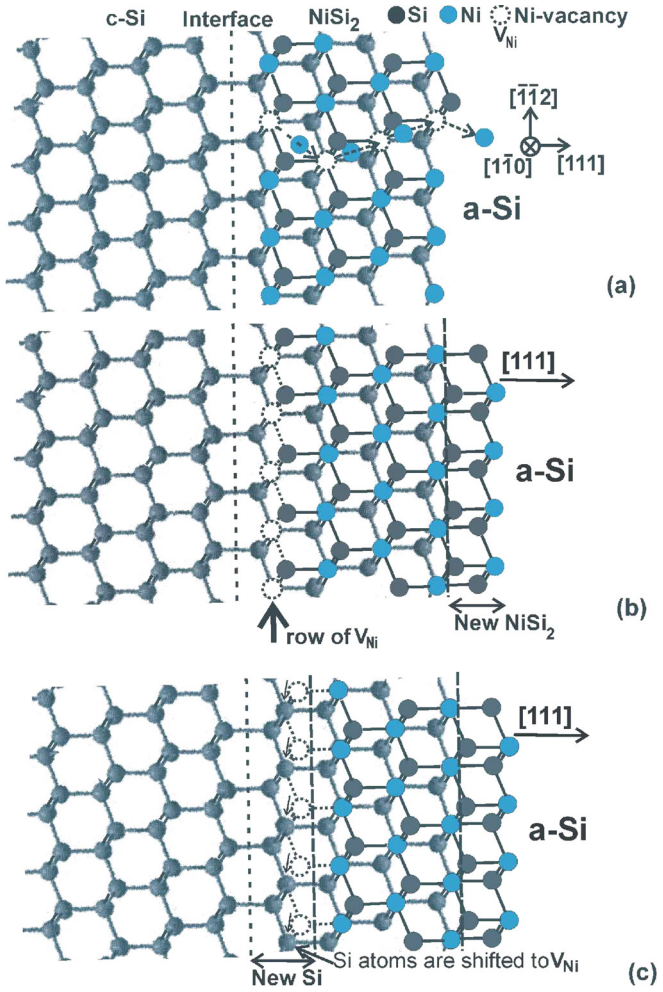

FIG. 1. Model of the MILC process: (a) Nickel atoms from the crystalline $NiSi_2$ diffuse to the a-Si leaving behind Ni vacancies, which are occupied by Si atoms migrating from the a-Si. (b) New $NiSi_2$ is formed in the front of the pad leaving behind crystalline Si in epitaxial relation with the $NiSi_2$ grain. (c) As the crystalline Si grows, the $NiSi_2$ pad moves forward loosing Ni, which dopes the c-Si.

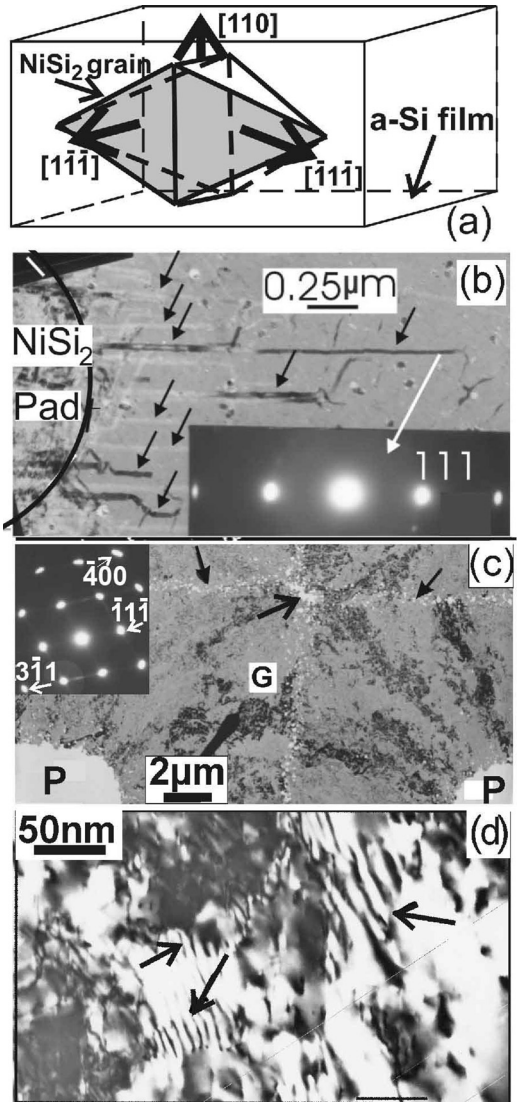

FIG. 2. (a) The most favourable case for Ni-MILC is when the [110] direction of an octahedral $NiSi_2$ grain is perpendicular to the a-Si film. In this case, four of the eight equivalent ⟨111⟩ directions are parallel to the film. (b) Bright field TEM micrograph from *in situ* crystallized a-Si film at 480 °C; needle-like crystallites emanate from the $NiSi_2$-pad denoted by arrows. In the inset, diffraction patterns from a crystallite reveal the growth along the [111] direction. (c) Low magnification TEM micrograph of poly-Si film crystallized by Ni-MILC after annealing at 600 °C for 1 h. The $NiSi_2$ pads are denoted by letter P. When the crystallization fronts from the neighbouring pads meet, holes due to $NiSi_2$ precipitates are formed, denoted by arrows. In the inset, the diffraction pattern from the grain, denoted by letter G, shows the strong preferred [110] orientation. (d) High magnification TEM micrograph from a grain. The grain consists of slightly misoriented partially overlapped sub-grains, resulting in the formation of moiré fringes of the rotational type, denoted by arrows.

have the form of regular octahedra, bounded by eight {111} faces having 0.4% lattice mismatch with Si. The Ni from the leading Si edge of the needle-like crystallite moves to a new leading edge, forming there a new nickel di-silicide precipitate to maintain the needle-like crystalline growth along one of the equivalent ⟨111⟩ directions, as schematically shown in Fig. 1. The most favourable case is when the [110] direction of the octahedral $NiSi_2$ grain is perpendicular to the a-Si film, because two ⟨111⟩ equivalent directions are parallel to the a-Si film, as schematically shown in Fig. 2(a). The Ni-MILC process was confirmed by *in situ* heating experiments in a Transmission Electron Microscope (TEM), and needle-like crystallites were formed at 480 °C, as shown in Fig. 2(b).[13] In this case, the needle-like grains can change direction to another equivalent ⟨111⟩ direction, which is also parallel to the plane of the a-Si film resulting in the formation of large grains exhibiting [110] preferred orientation, as shown in the inset of Fig. 2(c). Grains having their ⟨111⟩ directions inclined to the plane of the film also grow fast but soon reach the bottom or the top of the film and stop there.[13,14] The needle-like crystallites scan the a-Si film, switching the growth direction to all the possible ⟨111⟩ directions, which are parallel to the plane of the film retaining the [110] preferred orientation, until the entire area is crystallized.[13] The remaining narrow amorphous silicon gaps between the needle-like crystallites are crystallized by conventional SPC with the needle-like crystallites acting as crystalline seeds. In this way, a one-dimensional growth along [111] direction leads to two-dimensional crystallization. It is worth noticing that an amorphous silicon film exhibits more than 10 h incubation period for random nucleation at 600 °C.[14,15] In

contrast, the incubation time for Ni-MILC at 600 °C is zero, and nickel-induced-crystallization starts with the onset of the annealing. Moreover, the crystallization rate of Ni-MILC process is about 18 μm per hour, which is roughly 50 times faster than the standard SPC process.[16] The $NiSi_2$ clusters promote a faster crystallization and rule out the long incubation period, which is required for the formation of the first nuclei in a-Si. Therefore, well above 500 °C, both MILC and SPC run in parallel, and this case is discussed in Section III D.

The completion of the Ni-MILC process after annealing at 600 °C for 1 h in a two dimensional periodic array of $NiSi_2$ pads is shown in Fig. 2(c). The crystallization starts from the pads, forming V-shaped grains having [110] preferred orientation, as shown in the related Selected Area Diffraction (SAD) pattern in the inset of Fig. 2(c), which was taken from the grain denoted by letter G. When the crystallization fronts from neighboring pads meet each other, a wall of small holes is formed as shown by arrows in Fig. 2(c). These holes are attributed to the leading $NiSi_2$ precipitates, which were subsequently etched out by the HF solution during TEM sample preparation. The same happened with the $NiSi_2$ in the pads, which appear empty, denoted by letter P in Fig. 2(c). The small holes are located in the middle of the distance between the neighboring pads, proving that the growth rate from each pad is the same. As it is evident from Fig. 2(c), the grains exhibit a black and white mottle like contrast, which is a characteristic in mosaic structures. This is evident from the diffraction spots, which are arcs, like the $\underline{2}22$ in the inset of Fig. 2(c). This is also confirmed by the high magnification micrograph in Fig. 2(d), which reveals that the large grains consist of a high number of slightly misoriented sub-grains, about 60 nm in size. Moiré patterns of the rotational type are produced by the overlapping, slightly misoriented sub-grains, shown by arrows in Fig. 2(d). From the periodicity of the Moiré patterns, the degree of misorientation of the sub-grains was estimated, and misorientations up to 8° were measured.[14]

The driving force for the phase transformation is the reduction in free energy associated with the transformation of metastable a-Si to the stable c-Si.[10] More specifically, the chemical potential of Ni is lower at the $NiSi_2$/a-Si interface. This is the driving force for Ni to move toward a-Si in order to reduce free energy.

The MILC process starts at 400 °C; however, most of the MILC experiments presented in the literature were performed at the temperature range of 500 to 650 °C.[10–13] As far as we know, no systematic MILC studies were performed at the temperature range of 400 to 500 °C. Only Makihira *et al.*[17] performed experiments in this range, showing the formation of very long needle-like crystallites without the change of their growth direction. Even in this case, the structural characteristics and the mode of growth of these long whiskers were not studied. It is worth noticing that TFTs fabricated on such whiskers exhibit very good performance.[18]

In this work, we study the structural characteristics and the mode of growth of the whiskers grown by Ni-MILC at the temperature range of 413 to 521 °C using TEM. In this range, the crystallization is solely affected by Ni-MILC; on the contrary, at higher temperatures, the SPC contribution is significant.[12] Strong anisotropic Ni-MILC growth is observed at the temperature range of 400–450 °C. As far as we know, this is the first time where the structural characteristics of the pure Ni-MILC are studied without the involvement of SPC. The crystallization rate is strongly influenced by the distribution of the neighbouring $NiSi_2$ pads, and this long-range effect is discussed in detail in Section III C. The formation of nickel silicides and the crystallization of a-Si under limited and unlimited Ni supply conditions were also examined by *in-situ* experiments in TEM.

II. EXPERIMENTAL PROCEDURE

For the MILC *in situ* experiment under Ni limited source, a 3 in. (001) Si wafer was thermally oxidized so that a 200 nm thick SiO_2 buffer layer was formed. A 50 nm thick intrinsic a-Si film was deposited by Low-Pressure Chemical Vapour Deposition (LPCVD) at 500 °C using silane. Then, a 50 nm thick silicon oxide capping layer was deposited by Plasma Enhanced Chemical Vapour Deposition (PECVD). For the conventional Ni-MILC process, windows having different geometries at different distances were opened by lithography on the upper oxide protection layer. Specifically, windows with sides from 1 μm to 100 μm having different periodic distances were opened on the capping oxide layer, and subsequently a 15-nm-thick nickel film was deposited on top by vacuum evaporation, so that Ni pads were formed, and the substrate during Ni evaporation was kept at RT. The thickness of the Ni and Si films in the pads was chosen to be close to the $NiSi_2$ stoichiometry. Recently, a new, simpler, and faster method was proposed for the formation of Ni nanosize particles.[19] In order to observe the formation of $NiSi_2$, as well as the crystallization of the a-Si during the *in situ* annealing experiment in cross-section, TEM specimens were prepared by the Focused Ion Beam (FIB) technique.[20] This technique ensures that the area of interest is transparent to the electrons, in the present case the area around a Ni pad. A Philips CM20 TEM equipped with a heating holder was used for the *in situ* heating experiment. The temperature was measured by a thermocouple. The accuracy of the measured temperatures was tested by *in situ* phase transformations, which shows a temperature difference between the specimens and the thermocouple up to ±15 °C. High Resolution TEM (HRTEM) observations were subsequently performed on the annealed specimen using a JEOL 3010 JEM microscope equipped with Electron Energy Loss Spectroscopy (EELS) analysis. Analysis by EDS (Energy Dispersive System) was carried out in a FEI Tecnai 200 kV field emission gun STEM equipped with EDAX EDS for the characterization of the FIB prepared specimens.

Conventional Ni-MILC process was performed at low temperatures, in the range of 413 to 521 °C. For this purpose, the remaining wafer was annealed in nitrogen atmosphere at 250 °C for 10 min for the formation of $NiSi_2$ in the area of the windows. The remnant of the nickel layer was washed off by nitric acid; in this way, periodic $NiSi_2$ pads were formed. Subsequently, rectangular pieces, with dimensions 5 mm × 15 mm, were cut from this wafer and placed in

quartz ampoules, which were sealed in vacuum at 6×10^{-4} Torr and placed in furnaces for the low temperature annealing. The structural characteristics of the annealed specimens were studied by Plane View TEM (PVTEM) observations. Specimens for PVTEM observations were prepared by etching the upper-level protection SiO_2 layer and the SiO_2 buffer layer using HF and subsequently lifting off the Si film. Specimens suitable for cross-section TEM (XTEM) observations were also prepared at first by mechanical thinning the specimens down to 20 μm and then by thinning to electron transparency using Ar^+ ion milling at a low incident angle of 4°, in order to avoid amorphization during the ion thinning process.

For the unlimited Ni-MILC *in situ* annealing experiment in TEM, a Ni grid was used as Ni source. First, an a-Si film having a thickness of around 50 nm was deposited on a cleaved NaCl by magnetron sputtering. The film was removed from the substrate by dissolving the NaCl in water and transferred to the Ni grid. During this process, the formation of a native oxide ~2 nm on both sides of the film was inevitable.

III. EXPERIMENTAL RESULTS

A. *In situ* experiments

1. Limited Ni supply condition

The overall view of the cross-sectional FIB specimen near the edge of the window opened by lithography and etching before heating is shown in Fig. 3(a). Due to the 54 nm thick SiO_2 capping layer, nickel is in contact with the a-Si only in the window area, and a small over-etching of the SiO_2 capping layer at the window edge is observed. The thickness of the deposited Ni layer was sufficient to react with the underneath a-Si in the window area layer in order to turn it to $NiSi_2$ without leaving a large amount of non-reacted Ni in order to exclude the formation of $NiSi_2$ outside the window area (the pad). This is the concept of the limited Ni supply condition. A simple calculation shows that for the formation of $NiSi_2$, the thickness (h_{Ni}) of the Ni film must be related with the thickness (H_{Si}) of the underneath a-Si layer, with the following relation: $h_{Ni} = H_{Si}(a_{Ni})^3/(a_{Si})^3$, where a_{Ni} and a_{Si} are the lattice parameters of the Ni and Si unit cells, 0.35228 nm and 0.543 nm, respectively. For a 50 nm a-Si layer, the corresponding Ni film must be 12.9 nm; in practice, the deposited layer was slightly thicker, about 15 nm.

The formation of nickel silicide was already studied by *in situ* heating experiments by Thron *et al.*,[21] and it was shown that $NiSi_2$ is formed at temperatures as low as 280 °C. In this experiment, we focus to the formation of $NiSi_2$ in the window area and the start up of the Ni-MILC process at the edge of the pad.

The *in situ* heating was performed at the temperatures range of 250–650 °C. The first $NiSi_2$ grains were formed at the Ni/a-Si interface after *in situ* heating at 250 °C for 3 min, as shown in Fig. 3(b). As the time passes, the crystallization is extended in depth inside the a-Si, as is evident in the sequence of the micrographs in Figs. 3(c) and 3(d) taken, respectively, after 12 and 18 min. After 61 min, 25 nm of the

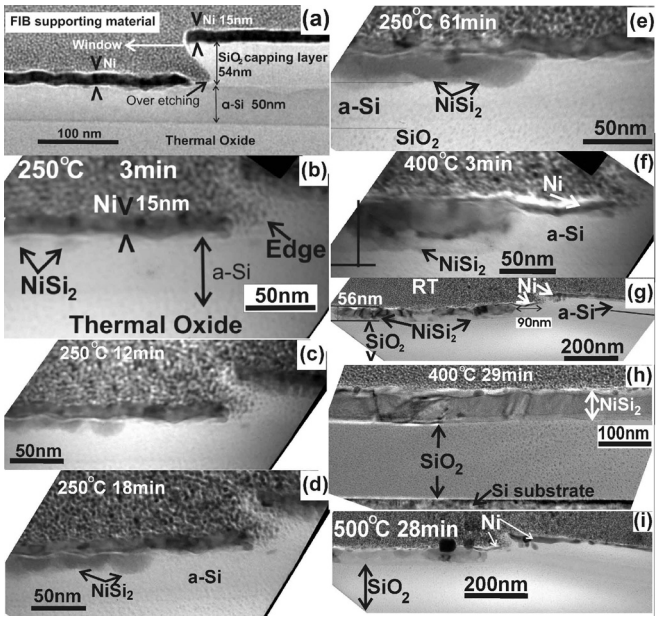

FIG. 3. XTEM micrographs of the FIB specimen taken during the *in situ* heating experiment. (a) The structure of the specimen at the edge of the window before annealing. (b) The same area after annealing at 250 °C for 3 min. (c) The same area after annealing at 250 °C for 12 min. (d) After annealing at 250 °C for 18 min. (e) The same after annealing at 250 °C for 61 min. (f) The same area after annealing at 400 °C for 3 min. (g) The overall view of the area around the edge of the window at low magnification after cooling down the specimen to RT. (h) An area of the window far from the edge after further annealing at 400 °C for 29 min. (i) The area around the window after annealing at 500 °C for 28 min.

a-Si was crystallized to $NiSi_2$, as shown in Fig. 3(e). The 15 nm thick Ni layer was only partly consumed, about 7.8 nm of the Ni layer was left; also, the formation of the $NiSi_2$ was not homogenous along the window, as shown in Fig. 3(e). Near the edge of the window and up to a distance of 87 nm from it, no $NiSi_2$ was formed; the Ni film along this distance remained intact. It is speculated that this is due to contamination related with the lithography for the window formation, which inhibits the reaction of Ni with the a-Si. Increasing the temperature to 400 °C, the remaining a-Si in the window was consumed forming $NiSi_2$ up to the thermal oxide within 3 min; in the same area, all the Ni, which was left after the annealing at 250 °C, was reacted and consumed, as shown in Fig. 3(f). The only exception was the 87 nm long a-Si zone from the edge of the window, which remained intact, although the Ni layer there was reduced. We speculate that there was a nickel migration to a neighbouring area for the formation of $NiSi_2$ there. Further heating for another 26 min did not produce any change, as shown in Fig. 3(g), suggesting that the formation of the $NiSi_2$ was already completed, and no lateral crystallization of the a-Si occurred because at this temperature the MILC process is very slow. The formation of the $NiSi_2$ inside the window, far from the edge, after annealing at 400 °C for 26 min, is shown in Fig. 3(h). The Ni was consumed, and the $NiSi_2$ touched the thermal oxide everywhere.

After increasing the temperature to 500 °C, Si crystallization occurred due to the MILC process; this is shown in Fig. 3(i), which was taken after *in situ* heating for 28 min.

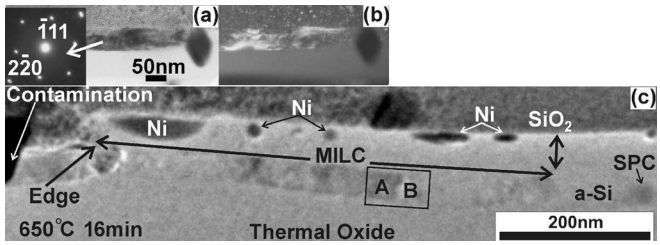

FIG. 4. (a) Bright field micrograph from a $NiSi_2$ grain in the window area. The related diffraction pattern is shown in the inset. (b) Tilted dark field micrograph from the same area taken from the ($\bar{1}11$) spot. (c) The overall view of the crystallized a-Si outside of the window.

The a-Si was laterally crystallized to a distance of 41 nm, having as marker the end of the nickel at the edge of the window. It is worth noticing that the already existing 6 nm thick Ni film did not react with a-Si. The two black grains that are shown by arrows in Fig. 3(i) are attributed to contamination of the protective layer (Pt and carbon), deposited at the beginning of the FIB process.[22] Low magnification Bright Field (BF) and Dark Field (DF) micrographs, taken from the area of the window after the *in situ* annealing, reveal the formation of grains that are extended to 50 nm in depth and 250 nm laterally, as shown in Figs. 4(a) and 4(b), respectively, with no traces of the Ni film left. The related Selected Area Electron Diffraction (SAED) pattern is shown in the inset of Fig. 4(a). From the SAED pattern, we can measure the inter-planar lattice distances with an accuracy of 1% using as reference the d-spacing of the single crystalline Si substrate. This ambiguity exceeds the 0.4% difference of the $NiSi_2$ and Si lattice parameters. Therefore, SAED patterns are insufficient to distinguish the Si and $NiSi_2$ compounds. However, considering that at this temperature, the MILC process is insignificant; it is safe to conclude that the grains are $NiSi_2$.

In order to remove any ambiguity, EDS analysis was performed, and Z-contrast images were taken, which confirmed the formation of $NiSi_2$ compound, and this is discussed in the next paragraph. Finally, the specimen was annealed at 650 °C for 16 min; during this period, the a-Si was crystallized by MILC to a distance of 620 nm from the edge of the window, as shown in Fig. 4(c). During this last annealing, no changes were observed in the already crystallized zone on the left side of the window. At this temperature, SPC also starts; therefore, small isolated c-Si islands were formed inside the a-Si, as shown on the right-end side in Fig. 4(c). The Ni layer over the SiO_2 buffer layer precipitated, forming large droplets of Ni in order to reduce the surface energy of the system and creating distortion of the SiO_2 capping layer, and the Ni granulates are always separated by an oxide layer from a-Si. Granulation of the Ni layer does not play any role in the standard MILC process because first it occurs only above 600 °C and second the non-reacting Ni after the formation of the $NiSi_2$ at the pads is washed off, as it is described in Section II.

The region shown in Fig. 4(c) was also investigated by EDS in a STEM equipped with a HAADF detector. In Fig. 5(a), the Z contrast image is shown with a dotted arrow inside the MILC stripe indicating the position of the line scan. Along this line, 20 EDS spectra were taken. The

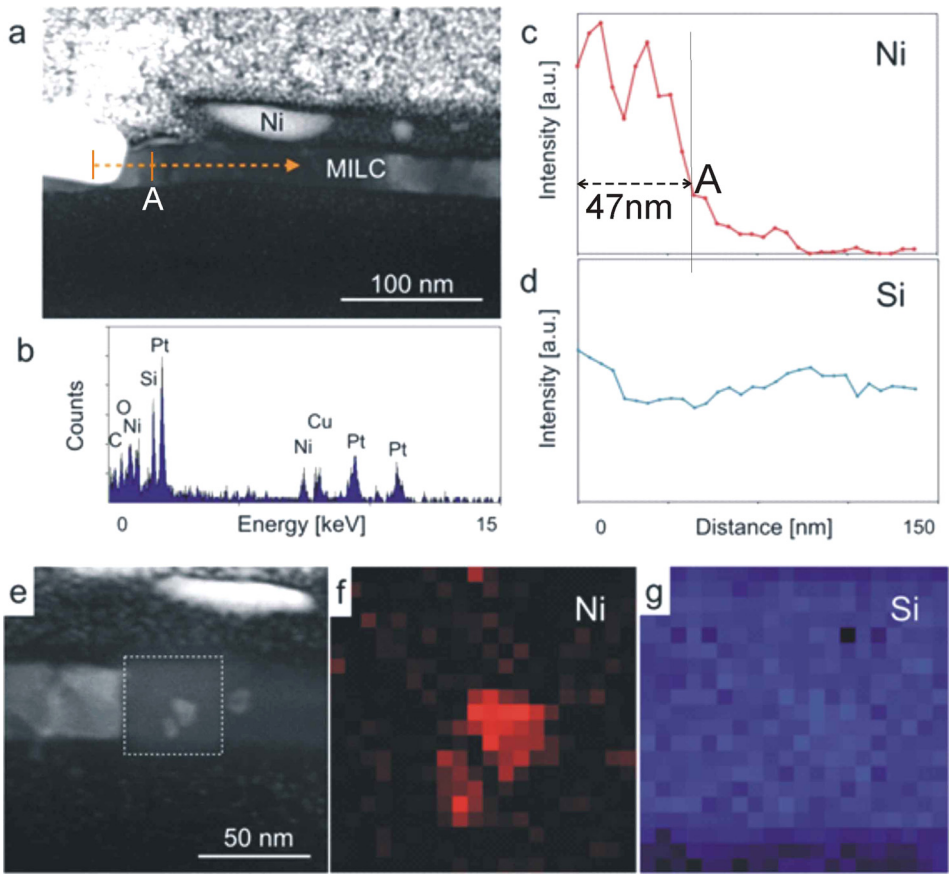

FIG. 5. Chemical composition study of the sample annealed at 650 °C. The arrow in (a) HAADF STEM image shows the EDXS line-scan measurement position. (b) EDXS spectrum recorded at the Ni-rich region. (c and d) Intensity profiles of Ni K edge and Si K edge extracted from the EDXS experiment. Dotted square in (e) HAADF STEM image showing EDXS map position. The extracted (f) Ni and (g) Si maps reveal Ni-rich crystals and homogenous Si distribution.

distribution of Si and Ni is presented in Figs. 5(c) and 5(d), respectively; for the EDXS elemental maps, the Ni K-lines ($K\alpha = 7.474$, $K\beta = 8.267$ keV) and the Si K-lines ($K\alpha = 1.74$, $K\beta = 1.837$ keV) were used. The Ni content is high in the window region where originally the Ni metallization was in contact with amorphous silicon, and first, this turned to $NiSi_2$ during annealing. As we leave the window region with the line scan, the Ni content is dropped, and pure silicon is measured. This is consistent with the fact that the MILC crystallized silicon does not contain nickel or at least it is below the detection limit of the apparatus. The Si content in Fig. 5(d) remains more or less the same because it corresponds to the a-Si that was initially deposited and had the same thickness inside and outside of the window.

Our next goal was to detect the $NiSi_2$ "seed" crystals that leave behind the crystallized silicon during the MILC process. For this purpose, two dimensional scans were carried out in the dotted square region shown in Fig. 5(e) in which two small grains are seen in front of the crystallized Si stripe. The Ni and Si maps are shown in Figs. 5(f) and 5(g). The Si distribution is very homogeneous in this map, while the two small crystals contain Ni as well, proving that we could detect and localize the $NiSi_2$ small crystals. We have not observed Ni pile up at the Si/thermal oxide buried layer interface, as it was reported by Zhonghe *et al.*,[23] because in our case, all the a-Si in the window was transformed into $NiSi_2$.

The grains grown by the MILC are relatively small of the order of 50 nm, as shown in Fig. 4(c). The orientation of some Si grains crystallized by the MILC process was studied by HRXTEM. Two grains denoted by letters A and B in Fig. 4(c) are shown at higher magnification in Fig. 6. Part of the area of the grain A is shown in the inset on the upper left hand-side in Fig. 6 at high resolution and part of the area of the grain B is shown in the upper right corner in the same figure. The observed lattice planes are not resolved well due to the radiation damage produced in the lattice by the FIB process. The noise in the related diffraction patterns was reduced by applying filtered Fast Fourier Transform (FFT) as shown in the insets denoted by IFFT (Inversed Fast Fourier Transform) in Fig. 6. For grain A, the (111) section is evident, revealing that the [111] direction is perpendicular to the plane of the figure. A preferential growth along this direction due to MILC is limited by the thickness of the FIB specimen, which does not exceed 60 nm. The corresponding IFFT is also shown on the low left corner in Fig. 6. Grain B in the same figure is observed in the (211) section as is evident from the masked FFT, which is shown on the upper right side in Fig. 6. The IFFT lattice image is also shown on the low right side in Fig. 6. In this case, the [11$\underline{1}$] direction is in the plane of the figure, but it is inclined to the long side of the FIB forming an angle of 16° with it; consequently, the MILC growth along this direction stops after 170 nm. It is worth noticing that the area of observation in a FIB specimen is three order of magnitude lower in respect of a standard PVTEM specimen. Therefore, it is very unprobable to see in a FIB specimen a whisker like the one shown in Fig. 2(b).

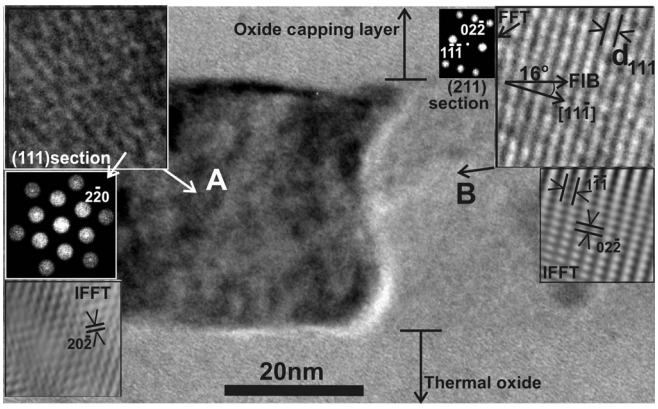

FIG. 6. High resolution micrographs from the grains A and B denoted by a rectangular shown in Fig. 5(c). Diffraction pattern from the grain A, after Fast Fourier Transform (FFT) processing, is shown in the inset at the left-side of the figure, together with the filtered lattice image after applying inverse FFT. The same is shown for the grain B in the insets at the right-side of the figure.

2. Unlimited Ni supply condition

In this experiment, a Ni grid was used as Ni source for our annealing experiment. First, an a-Si film was deposited on cleaved NaCl by magnetron sputtering. The film thickness was around 50 nm. The film was removed from the substrate by dissolving the NaCl in water and transferred to the Ni grid for *in-situ* heat treatment. During this process, the formation of native oxide of ~2 nm on both sides of the film, and <1 nm on the Ni grid, is expected. These oxides inhibit the reaction at low temperatures during the *in situ* heating. Silicide formation started at 600 °C near the grid bars. The growth front was moving in small abrupt steps, and in each step, a small grain was transformed to dark contrast silicide grains about 10 nm in size, as can be seen in Fig. 7(a). The polycrystalline structure behind the growth front has elongated grains reaching to the growth front. Most of the grains had a width between 30 and 100 nm. A second growth front appeared behind the first one with about 300–1000 nm separation. Behind the second growth front, larger grains appeared. These are also elongated grains mostly reaching to the growth front (the second front), and their width is 200–400 nm (Fig. 7(b)). SAED patterns showed that the fine grained phase is mostly $NiSi_2$ (inset at the lower right-hand corner in Fig. 7(b)), and the large grains are Ni_3Si_2 (inset at the upper left-hand corner in Fig. 7(b)). The SAED results were confirmed by performing qualitative EELS Ni elemental mapping of the annealed film, as shown in the micrograph on the lower left-hand corner in Fig. 7(b). The Ni content of the two crystalline phases clearly differ; additionally, no gradient is seen in the three phases (Ni_3Si_2, $NiSi_2$, and amorphous Si) on the map. We did not observe the NiSi phase, which is a stable phase with a Ni content between the two phases.[24] The Ni concentration changes in steps at the growth front.

B. Low temperature long time annealing

The patterned wafer described in Section II was used for the formation of $NiSi_2$ pads as already described. Pads having different periodicity and size were used as shown in the

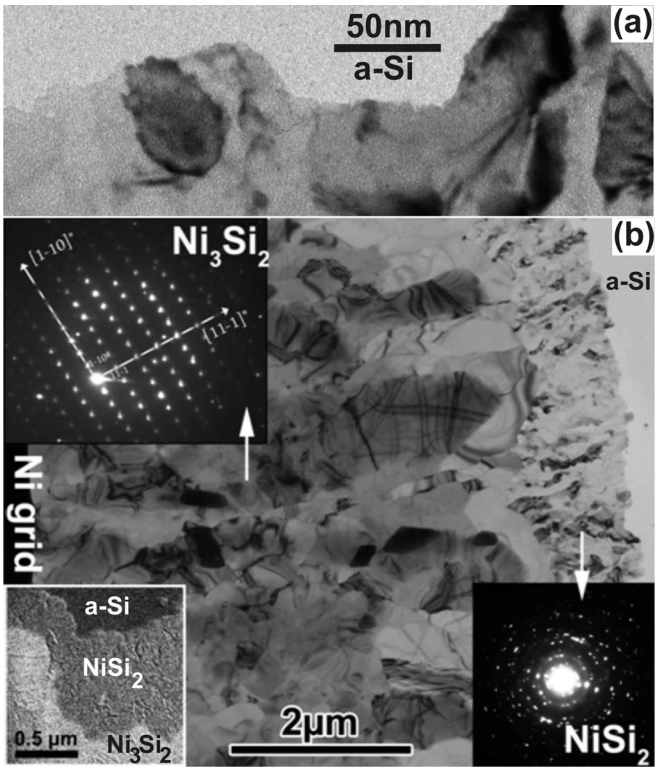

FIG. 7. Silicide formation under unlimited Ni supply condition. (a) Silicide grains formation at 600 °C. (b) Overall view of the crystallized area after cooling down the specimen to the room temperature. The inset at the upper left-hand side shows the diffraction pattern from a Ni_3Si_2 grain. The inset at the lower right-hand side shows diffraction pattern from small polycrystalline $NiSi_2$. The inset at the lower left-hand side is the EELS Ni elemental mapping of the film.

Optical Microscope (OM) micrograph in Fig. 8. Pieces from this wafer were annealed in vacuum at different temperatures, in the range of 413–521 °C, for 3 to 32 days. Specifically, the following low temperature annealing experiments were performed.

1. Annealing at 413 °C for 11Ds (days) and 32Ds

Tetragonal periodic $NiSi_2$-pads with sides of about 70 μm are shown in Fig. 8. Between them, there are smaller ones, 10 μm in size, denoted by letters A and B. After annealing at 413 °C for 11Ds, the a-Si around the large pad was crystallized to a distance of 3.5 μm. Part of the crystallized zone is shown in the lower part of the optical micrograph in Fig. 9(a). The crystallized zone is very irregular, with long whiskers emanating from the (a-c) interface. Some of these whiskers exceed 10 μm, as shown in the inset at the lower left side in Fig. 9(a). TEM observations reveal that the whiskers have a width of the order of 200 nm; far below, the resolution of the OM, therefore, could not be resolved on optical images. However, they give a faint contrast by dispersing the light due to their length. The crystallization around the small pad (A) retards in respect to the large pad, and it is asymmetric as shown in Fig. 9(a). The asymmetry was created by the influence of the neighbouring pads, and it is attributed to the long-range interaction in the MILC process, and this effect is discussed in Section III C. The crystallization around the pads was significantly extended after 32Ds annealing, as shown in Fig. 9(b), suggesting a rather constant growth rate within the experimental error. The crystallization rate increases with the size of the pad, as it is evident by comparing the crystallization front around the small pad (A) with respect to the large pad in Figs. 9(a) and 9(b). This is also evident by comparing three rows of small pads with different sizes annealed under the same condition, namely, at 413 °C for 11Ds, as shown in Figs. 9(c)–9(e). The structure of a pad after annealing is shown in the low magnification TEM micrograph in Fig. 9(f) (further details of the same pad are shown in Fig. 16(c) and will be discussed later).

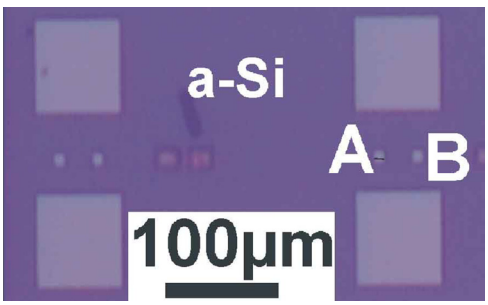

FIG. 8. Optical micrograph in reflectance mode of the tetragonal periodic $NiSi_2$-pads before annealing. Small, 10 μm pads are denoted by A and B, also 74 μm large pads are shown.

The crystallization rate versus the size of the pads at constant annealing temperature and time is exponential. This is shown in the plot in Fig. 9(g) for annealing temperature 413 °C and time 11Ds. This can be explained by considering that MILC mediated by the formation of $NiSi_2$ in the head of the crystallized front and a small Ni portion was trapped due to the Ni solubility in Si. Although this is very small, under limited Ni supply condition, the available Ni after long annealing is exhausted and the MILC process retards. Therefore, larger pads ensure higher crystallization rate under the same annealing temperature and time. It was shown by Jin *et al.*[23] that in Ni-MILC, at 500 °C, the crystallization is almost constant for the first 20 h and then is progressively reduced. The exhaust of Ni during the MILC readily explains this behaviour.[25] In contrast, in our long annealing experiment at 413 °C for 11 and 32 Ds, shown in Figs. 9(a) and 9(b) respectively, the crystallization rate is almost constant. This discrepancy is expected because at this low temperature the crystallization rate is more than one order of magnitude lower than at 500 °C. Therefore, the consumption of Ni is insignificant, and consequently, the rate remains constant for this long annealing time.

The crystallization rate is progressively reduced versus annealing time at higher temperatures, for example, in the 3 mm long $NiSi_2$ bar after annealing at 590 °C for 1, 2, 3, and 4 h, as shown in Fig. 10. The crystallization distance and rate versus time of the c-Si front from the $NiSi_2$ bar are shown in Fig. 10(e). The crystallization around two neighbouring A and B pads is also shown for comparison in Figs. 10(a)–10(d). The crystallization rate at the Ni-bar is significantly higher than in pads A and B due to the different geometry and the higher Ni content in the bar, as it was predicted by Qin *et al.*[26] In MILC, the $NiSi_2$ front moves into the a-Si

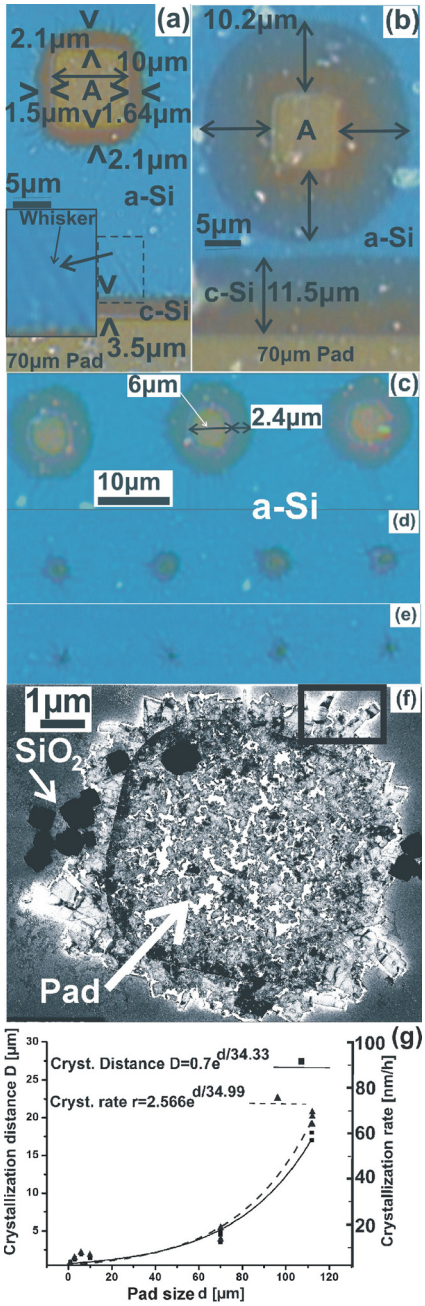

FIG. 9. Annealing of the $NiSi_2$ pads at 413 °C; at this temperature, crystallization occurs only due to MILC and no SPC process is involved. (a) Optical micrograph from the crystallized Si around the 10 μm pad A, also at the 70 μm large pad, after annealing for 11Ds. Whisker emanating from the crystallized area of the large pad is shown at higher magnification in the inset. (b) Crystallization around the same pads after 32Ds annealing. (c) Crystallization around 6 μm pads after annealing for 11Ds. (d) Crystallization around 3 μm pads after 11Ds. (e) Crystallization around 1 μm pads after 11Ds. (f) TEM micrograph from a 6 μm pad after 11Ds annealing. The microstructure of crystallized Si outside the pad is evident. The area denoted by the rectangular at the up right-side of the figure is shown at higher magnification in Fig. 17(c). (g) Plots of crystallization distance and crystallization rate versus pad size after annealing for 11Ds, both are exponential.

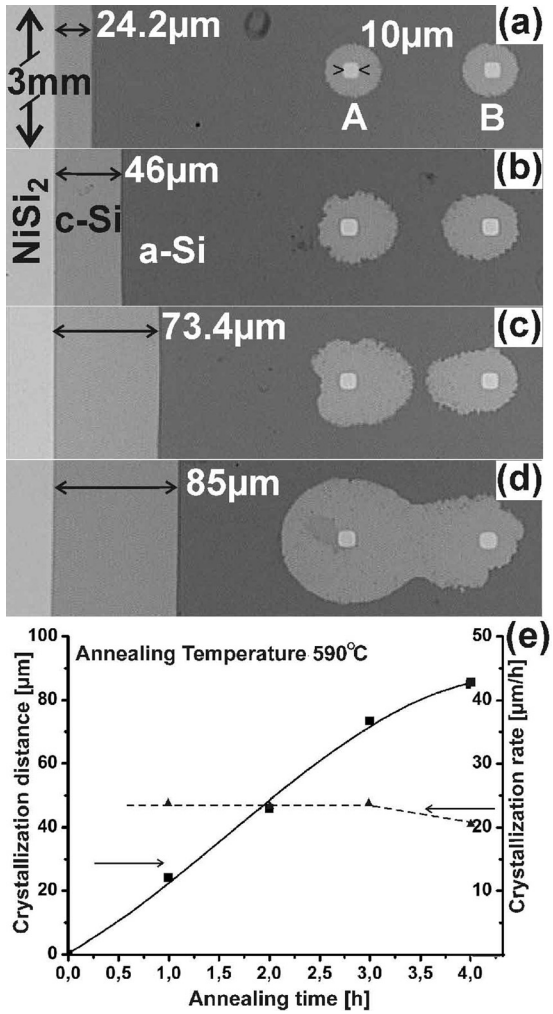

FIG. 10. Optical micrographs showing the crystallization fronts of a 3 mm long bar, also the crystallization around two 10 μm pads A and B after annealing at 590 °C. (a) For 1 h, (b) 2 h, (c) 3 h, (d) 4 h. (e) Plots of crystallization distance and rate versus annealing time of the a-c Si front from the $NiSi_2$ bar. Decline of the growth rate is observed after long time annealing due to nickel consumption.

leaving in the crystallized silicon about 0.08 at. % Ni, which replaces the Si atoms.[12,27] The concentration of crystalline Si is 5×10^{22} atoms cm^{-3}. Therefore, the Ni concentration in the crystallized Si is $8 \times 10^{-4} \times 5 \times 10^{22}$ cm^{-3}, almost one Ni atom per 10^3 Si atoms. Consequently, as the length of the c-Si increases, the thickness of the $NiSi_2$ front is reduced, and after a distance, the growth ceases.[22] However, the crystallization in the pads A and B in Fig. 10 is more complicated, and it is strongly anisotropic due to long range interaction. This effect is discussed in Section III C.

The inhomogeneous crystallization around the pads is more pronounced as their size and temperature are reduced. This is evident in the set of the 1 μm pads that were annealed at 413 °C for 32Ds, where whiskers up to 23 μm long were formed around the pads, as shown in Fig. 11(a).

Contamination plays a significant role in the MILC process, especially at low temperatures. This is evident in the set of the 36 pads, as shown in Fig. 11(b). The crystallization around the pads retards progressively from the right to the left and from the top to the bottom in this set. Contamination is more pronounced as the size of the pad is reduced. It is speculated that this is related to the etching process for opening the windows, as we have seen in the *in situ* experiment in Fig. 3(f). Consequently, the role of contamination at the rim of the pads becomes more decisive as their diameter is

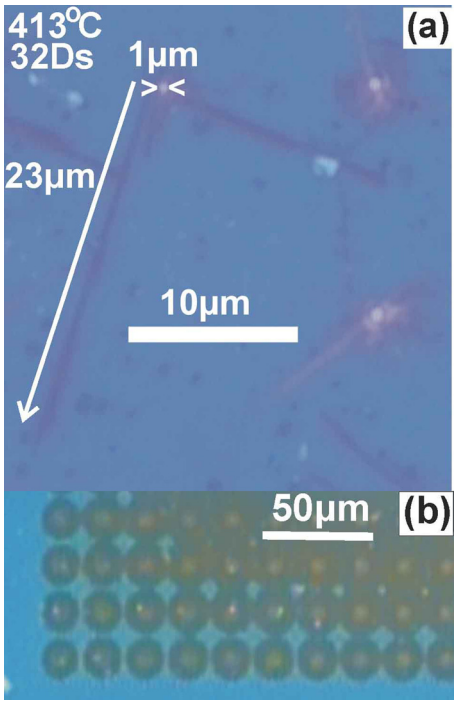

FIG. 11. Optical micrographs from specimens annealed at 413 °C for 32Ds. (a) The crystallization is very inhomogeneous when the pads are very small, and very long whiskers are frequently formed. (b) This set of $NiSi_2$ pads was formed and treated under the same conditions; however, due to contamination, significant differences in the crystallization rate are observed from right to the left and from the top to the bottom.

reduced. Nevertheless, as we have seen in the *in situ* experiment in Section III A 2, contamination due to native oxides is an obstacle for MILC, which starts only above 650 °C.

2. Three days (3Ds) annealing at 442, 454, 492, 512, and 521 °C

In this experiment, we have studied the evolution of the MILC at these temperatures for the same annealing time in pads with size of 6, 3, and 1 μm. The crystallization of these pads after 3Ds annealing at these temperatures is shown in the OM micrographs in Fig. 12. From this figure, it is evident that the a-c interface becomes smoother as the temperature and the size of the pads increase. At 492 °C, the a-c front is very smooth for the 6 μm pads, as shown in Fig. 12(f). In contrast, in the 1 μm pads, it remains discontinuous, as shown in Fig. 12(g). Above 512 °C, the a-c front around all pads is smooth, as shown in Figs. 12(h) and 12(i).

The activation energy of crystallization versus the size of 6, 3, and 1 μm pads was calculated by the logarithm plot of the crystallization rate r versus 10^3/T, where T is the absolute temperature, and the results are shown in Fig. 12(j). Pads with sizes 6, 3, and 1 μm are denoted by letters A, B, and C, respectively. The log(r) versus 10^3/T describes the Arrhenius equation of the crystallization process for the pads A, B, and C, respectively. The parameters of these lines after best fitting are given in Fig. 12(j) (low left-side), and from their slopes, the activation energy was calculated. For pad A, the slope is $9.61801 = E_A \times 10^{-3} \times \log(e)/k$, where $k = 8.63 \times 10^{-5}$ eV/K, and $\log(e) = 0.434294$; therefore, the

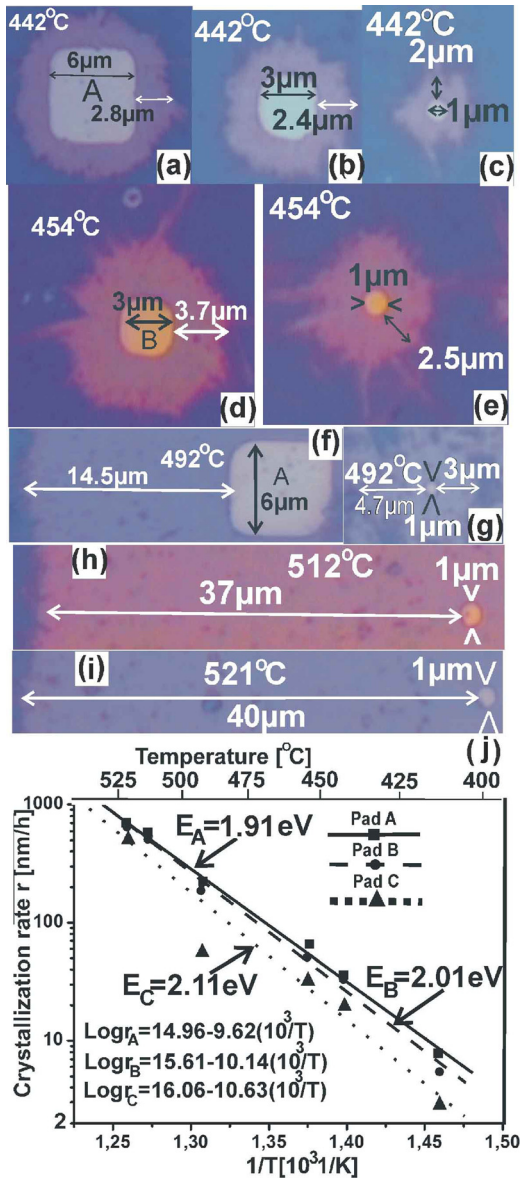

FIG. 12. Optical micrographs showing the crystallization around pads that were annealed for 3Ds in the range of temperature from 442 to 521 °C. The crystallization changes from very inhomogeneous at low temperatures and small pad size to very homogeneous at high temperatures and large pad size. (a) Pad size 6 μm, annealed at 442 °C. (b) Pad size 3 μm, annealed at 442 °C. (c) Pad size 1 μm, annealed at 442 °C. (d) Pad size 3 μm, annealed at 454 °C. (e) Pad size 1 μm, annealed at 454 °C. (f) Pad size 6 μm, annealed at 492 °C. (g) Pad size 3 μm, annealed at 492 °C. (h) Pad size 1 μm, annealed at 512 °C. (j) Pad size 1 μm, annealed at 521 °C. (k) Arrhenius plots of the growth rates for pads having size 1, 3, and 6 μm.

activation energy is $E_A = 1.91$ eV. For the pad B, $E_B = 2.01$ eV and for pad C is $E_C = 2.11$ eV. Within the experimental errors, the activation energy is independent of the size of the pads. It is evident that the activation energy for MILC is significantly lower than that of the conventional SPC, which is around 4 eV.[28] The pre-exponential factor (a) in Arrhenius equation is significantly different for the pads A, B, and C, $a_A = 0.915 \times 10^{15}$, $a_B = 4.05 \times 10^{15}$, and $a_C = 11.62 \times 10^{15}$, respectively. This is related to the frequency of the reaction, and the difference is attributed to the different Ni content in the pads.

C. Long range interaction

The isolated pads exhibit a symmetrical radial crystallization; however, if in the vicinity of the pad another Ni-pad exists, the crystallization becomes inhomogeneous, strongly depending on the relative position of the Ni pads. This is the case with pads A and B, as shown in the OM micrograph in Fig. 10. After annealing at 590 °C for 1 h, the crystallization front around the pads is slightly enhanced at the inner side of the pads, with respect to the outer sides, as shown in Fig. 10(a). The asymmetric crystallization is greatly enhanced after 2 h annealing, as shown in Fig. 10(b). After 3 h annealing, crystallization occurred mainly at the inner side, Fig. 10(c). Finally, after 4 h, the two inner fronts touch each other, and the crystallization front at the outer side of pad B was only slightly advanced; on the contrary, the outer side of pad A is significantly advanced, as shown in Fig. 10(d). This difference is attributed to the influence of the advanced front of the crystallized bar, which influences the crystallization front of pad A.

There are two possible mechanisms for the long-range interaction:

(a) The local increase of the temperature due to heat release by the amorphous-crystalline transformation.
The amorphous to crystalline transformation in silicon films is exothermic, and the heat released per unit area of the film is proportional to the film thickness. A part of this heat is dissipated to the surroundings through the surface of the film, and the remaining increases the temperature of the film close to the crystallized area. Thick or thin films have the same free surface and consequently roughly the same losses. Therefore, a thicker film is expected to increase the temperature in the a-c interface more than a thin one, namely, the crystallization rate would depend on the thickness of the film. The crystallization rates in two a-Si films with thickness 50 and 100 nm, respectively, annealed simultaneously were measured. For this purpose, tetragonal 20 μm × 20 μm pads of a-Si 50 nm thick were formed by lithography denoted by letter A in the inset of Fig. 13. Subsequently, a second a-Si film having the same thickness was deposited on top, as denoted by letter B in Fig. 13. In the area of the two overlapping films, the total thickness was 100 nm and out of this only 50 nm, as it is shown schematically in cross-section in the inset of Fig. 13. Then, a 50 nm thick silicon oxide capping layer was deposited by PECVD. For the Ni-MILC process, long rectangular windows were opened in the oxide capping layer and a 15 nm thick nickel film was deposited on top so that Ni pads were formed. The wafer was annealed at 250 °C for 10 min for $NiSi_2$ formation. This specimen was annealed at 590 °C for 30 min, and the result is shown in the PVTEM micrograph in Fig. 13. In both sides (A and B), the crystallization rate was the same revealing that the crystallization rate is not affected by the thickness of the film, at least in this rage of thickness. Therefore, heat release during crystallization does not affect the MILC process.

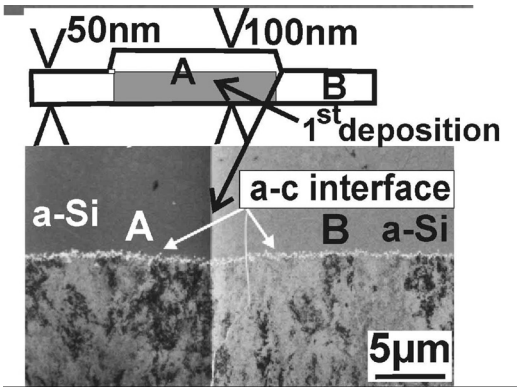

FIG. 13. The plane view TEM micrograph shows that the crystallization rate is independent of the thickness of the film. Letters A and B denote 100 nm and 50 nm thick films. The inset shows schematically in cross-section the thickness of films A and B. The film was annealed at 590 °C for 30 min, and the a-c interface has advanced at the some distance independent of the thickness of the films.

(b) Due to Ni diffusion into the a-Si ahead of the advancing a-c front.
The Ni concentration in the a-Si in the front of the advancing a-c interface must reach a critical concentration before the onset of the crystallization there. This behaviour agrees well with other observations in metal-semiconductor multi-layers where metals, such as Ti, Ni, Co, Zr, and Pt, induce crystallization in Si, by metallic-semiconductor elements inter-diffusion. Thus, an amorphous mixture is produced prior to the onset of the crystalline phase formation by the solid state reaction.[29–31] The driving force for the formation of this intermediate amorphous compound before the onset of crystallization is the large negative free energy of mixing between Ni and Si at a maximum rate.[32,33] Therefore, the long range interaction is attributed to the Ni diffusion into the a-Si before the onset of the Ni-MILC, which starts when the Ni in the a-Si reaches a critical concentration. The Ni concentration can reach this critical point faster when independent Ni sources contribute to the same a-Si area of interest. This was confirmed by SIMS analysis, which reveals that Ni concentration in a-Si is about 0.01% the Si atomic percent.[12] The long-range interaction permits the enhancement of the crystallization rate along certain direction by proper arrangement of the $NiSi_2$ pads.

D. Preferred orientation of the grains crystallized by Ni-MILC at 590 °C

The critical role of the Ni concentration in the a-Si for the initiation of the MILC process is shown in Figs. 10(b)–10(d). The crystallization at the outer part of the pad A has ceased after 2 h annealing due to Ni depletion, establishing slow SPC, as shown in Figs. 10(b) and 10(c). However, the MILC process is restored as soon as the advancing crystallization front from the $NiSi_2$ bar reaches the pad due to Ni enrichment of the a-Si from the approaching crystalline front from the bar, as shown in Fig. 10(d).

The long-range interaction affects not only the crystallization rate but also the mode of growth. As it was confirmed by *in situ* experiments,[13] above 500 °C, MILC and SPC coexist. This is also evident by the increase of the activation energy at higher temperatures due to the contribution of the SPC.[12] The degree of the contribution of MILC and SPC depends on the annealing conditions and can change during annealing. For example, Fig. 14(a) is a low magnification PVTEM micrograph of two Ni-pads A and B after 1 h annealing; the asymmetric crystallization around the pads is evident. Close to the pads and up to a distance of 6 μm, V-shaped grains were formed as already described in Section I A, typical of a MILC process. At larger distances, significant differences are observed in the microstructure at the inner and outer sides of the pads. These differences are shown by the PVTEM micrographs in Figs. 14(b) and 14(c), which were taken from the areas (1) and (2) at the inner and outer part of the pad B near the a-c interface. In area (1), the crystallization proceeds with the formation of long needle-like crystallites with $NiSi_2$ precipitates at the leading edge, denoted by arrows in Fig. 14(b) and having [110] preferred orientation, revealing a typical MILC process.[13,14] In contrast, the crystallized front at the outer side area (2) of the pad B is different. No needle-like crystallites or holes due to advancing leading $NiSi_2$ grains were observed, Fig. 14(c), suggesting Ni depletion conditions. The crystallization resembles SPC process, where the [111] preferred orientation prevails. The [111] preferred orientation is attributed to the strong heterogeneous nucleation at the Si/SiO_2 interface and the anisotropic growth of Si.[6,34,35] The difference in the mode of growth in area (1) and (2) is attributed to the long-range interaction, which ensures a higher level of available Ni at the inner side, area (1) of the pad.

It is worth noticing that cracks were formed around the pads, during the TEM specimen preparation after etching the SiO_2 buffer layer by HF and lifting off the film. The cracks are very close to the a-c front, as shown in Fig. 14(a). It is speculated that this is the result of strain deformation due to the small volume change during the a-c transformation.

The change of the preferred orientation from [110] for pure MILC to [111] for pure SPC occurs during the crystallization by progressive rotation of the small sub-grains shown in Fig. 2(d). It occurs by successive tilt of the sub-grains along a common crystallographic axis, which lies on the plane of the film. This is shown in the sequence of the micrographs in Fig. 15. Thus, Fig. 15(a) is a DF micrograph taken from the $02\underline{2}$ spot, by placing the selected area aperture in the area K. This is a typical diffraction pattern of the $(\bar{1}11)$ section, shown in the inset of Fig. 15(a). A large area is diffracting strongly, as shown in Fig. 15(a). However, this is not a single grain, since only part of the grain is diffracting strongly with the 220 spot, as shown in Fig. 15(b), revealing that we are dealing with a bi-crystal having as common

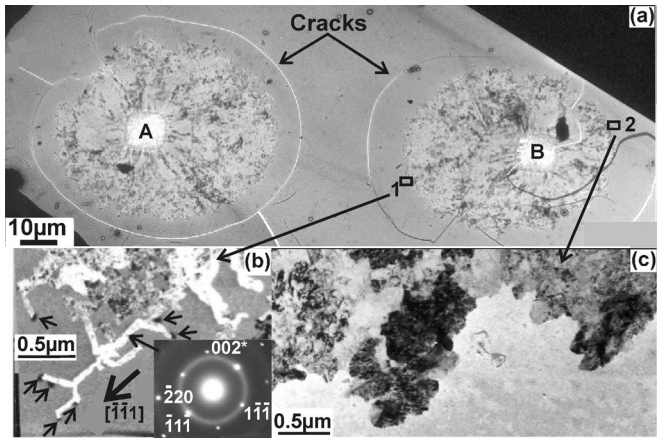

FIG. 14. Plane view TEM micrographs of a film crystallized after annealing at 590 °C for 1 h. (a) Overall view of the $NiSi_2$-pads A and B and the crystallized area around them. Appearance of cracks around each pad very close to the a-c front is evident. (b) Dark field (DF) TEM micrograph taken from the area denoted by letter 1 in figure (a) at the inner side of pad B. The crystallization mediated by the formation of needle-like crystallites, which are characteristic of the MILC process. Holes appearing black in DF, at the tips of the needles, denoted by arrows are attributed to the $NiSi_2$ grains at the tips of the whiskers, which were etched off in HF during the TEM specimen preparation. The related diffraction pattern shown in the inset confirms the preferred [110] orientation. (c) Bright field TEM micrograph taken from the outer side of the pad B, denoted by number 2 in figure (a). No needle-likes crystallites are observed in this area resembling conventional SPC process.

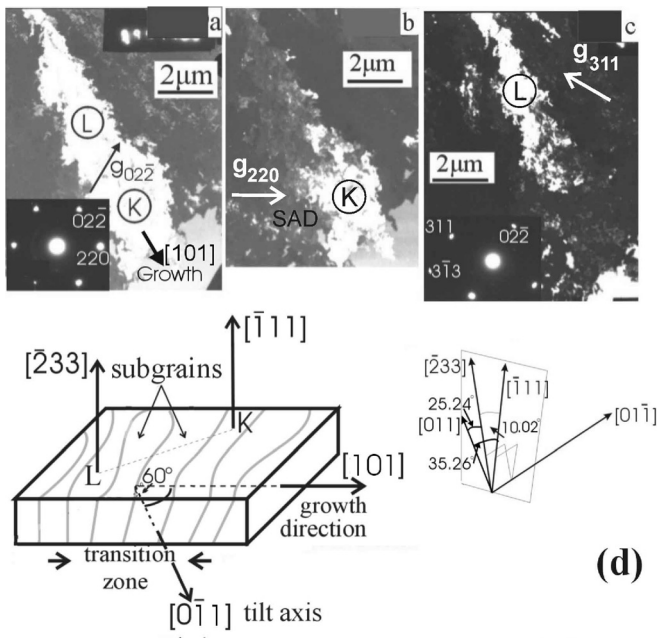

FIG. 15. TEM micrographs show the change of the preferred orientation of the grains occurring by progressive rotation of the sub-grains during MILC due to Ni consumption. (a) DF micrograph taken from $02\bar{2}$ spot that shows a long grain. The related diffraction pattern was taken by placing the Selected Area (SA) aperture at the place K, corresponding to the $(\bar{1}11)$ section, see the inset. (b) DF micrograph from the same area keeping the SA aperture at the same place and taking as operating reflection the 220 spot. Now only the half of this grain is diffracting, revealing that this is not a single grain but a bi-crystal having the $02\bar{2}$ as common reflection. (c) For confirmation, a DF micrograph was taken by placing the SA aperture in the area denoted by letter L. This area has different orientation exhibiting the $(\bar{2}33)$ section, as shown in the inset. The micrograph was taken from the non-common reflection 311, now the other half of the grain is diffracting strongly. (d) The characteristic feature of this bi-crystal is the absence of a defined grain boundary, the change of the orientation is progressive. This is shown by the schematic representation of the sub-grains in the area between L and K. These sub-grains are rotated progressively around the common [01] axis for about 10°. The corresponding crystallographic directions are shown in the inset.

reflection the 022; this is confirmed by the DF micrograph in Fig. 15(c). The area denoted by letter L corresponds to the (233) section, having with the section (111) the common 022 reflection, as shown in the inset of Fig. 15(c). This is evident by taking a DF micrograph from the non-common reflection 311. Now, only the upper half of the grain (area L) is diffracting strongly, as shown in Fig. 15(c). Therefore, the grains with sections (111) and (233) are rotated around the common axis [011] by 10°. The tilting from the (233) to the (111) section occurs progressively within a distance of 1 μm, as schematically shown in Fig. 15(d). The absence of a sharp grain boundary (GB) in this bi-crystal is explained by the existence of an intermediate transition zone as it is evident from Figs. 15(b) and 15(c), where the contrast fades progressively. The appearance of grains having the not so common [233] orientation is considered as the precursor to the transition from the Ni-MILC to the standard SPC mode of growth. This explains the relatively high percentage of grains with [233] preferred orientation at the a-c interface after a long annealing. The driving force for this transition is the reduction of the free energy of the system by changing from the amorphous to the crystalline state at a maximum rate under Ni depletion.

E. Structural characterization of the whiskers crystallized at 413 °C

1. Orientation of the whiskers

A PVTEM low magnification micrograph of a tetragonal 5.8 μm × 5.8 μm $NiSi_2$ pad with rounded corners is shown in the BF and DF micrographs in Figs. 16(a) and 16(b). The related SAD pattern, which was taken from the pad, is shown in the inset of Fig. 16(b). The diameter of the aperture for SAD was 0.8 μm, and the (111), (220), and (311) diffraction rings are observed. It is impossible to distinguish the Si and $NiSi_2$ rings due to the very small misfit between them. The DF micrograph in Fig. 16(b) was taken by placing the objective aperture (OA) in the (111) diffraction ring. Due to the coincidence of the Si and $NiSi_2$ rings, we observe strongly diffracting grains inside the pad, which belong to $NiSi_2$, as well as outside of it which belong to the crystallized Si. The latter is at least three times larger, in respect to the former not exceeding 150 nm. The generation of the Si crystallites from the borders of the $NiSi_2$ pad is shown in the higher magnification micrograph in Fig. 16(c), which was taken from the delineated area in the low magnification micrograph in Fig. 9(f). Three whiskers are emanating from the edge of the $NiSi_2$ pad, denoted by letters A, B, and C. From them, A and B are in the section (112), having the same orientation as revealed by the corresponding SAD patterns, suggesting that they originated from the same $NiSi_2$ grain. The crystallographic section of whisker C is (110), as shown in the related SAD. None of the whiskers has the [111] crystallization direction as should be expected according to the standard MILC process. Whiskers A and B grow close to [131] direction and whisker C grows close to [001]. The Ni-MILC process at 413 °C results in the formation of whiskers in several crystallographic directions. Examples are given in Figs. 16(d) and 16(e); in this last case, two whiskers having the same crystallographic section are crystallized in different directions. It is concluded

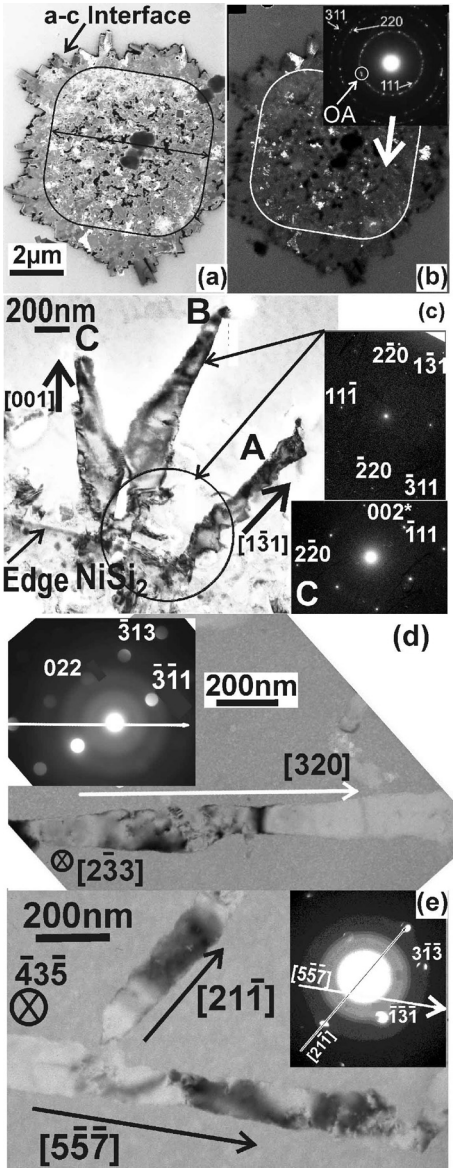

FIG. 16. TEM micrographs from specimens annealed at 413 °C for 11Ds. (a) BF from a $NiSi_2$ pad and the crystallized Si. (b) Tilted DF from the same area. The related SAD is shown in the inset. The TEM micrograph was taken by placing the objective aperture (OA) in the 111 ring shown by an arrow in the inset. (c) High magnification micrograph from crystallized Si delineated by a rectangular in Fig. 9(f). Three Si whiskers denoted by letters A, B, and C emanate from the $NiSi_2$ pad. The A and B are in the (112) section as the related SAD pattern reveals in the inset. Their crystallization direction is close to [131]. The whisker C is in (110) section and is crystallized along the [001] direction as the corresponding SAD shows. (d) A long whisker in the (233) section, which was crystallized along the [320] direction. (e) Two whiskers having the same (435) section, which were crystallized along the [211] and [557] directions, respectively.

that the requirement for the ⟨111⟩ preferred orientation is not a necessity for Ni-MILC process in the range 413–500 °C. This exclusion explains the easy formation of whiskers in this range of temperatures, with the only requirement remaining, the whiskers to be parallel to the plane of the film.

2. Ingrain defects in whiskers crystallized at 413 °C

Another feature of the whiskers shown in Fig. 16 is the low density of the ingrain defects and the absence of the

mottle-like contrast being characteristic for the mosaic structures, which is observed in crystallites grown by MILC at 600 °C, as shown in Fig. 2(d), also in Fig. 14. For comparison, the whisker shown at high magnification in Fig. 17(a) was grown at 413 °C having the [110] preferred orientation. No moiré patters or misoriented sub-grains are observed, as is the case of grains crystallized at 600 °C, shown in Fig. 2(d). The quality of this whisker was also confirmed by HRTEM, as shown in Fig. 17(b). The only highly disturbed area is the tip, where the $NiSi_2$ reactive grain boundary advances into a-Si. Nickel EELS mapping of this area reveals a high Ni concentration at the head of the whisker, as shown in the inset of Fig. 17(a). The high magnification micrograph in Fig. 17(c) and the related HRTEM in the inset

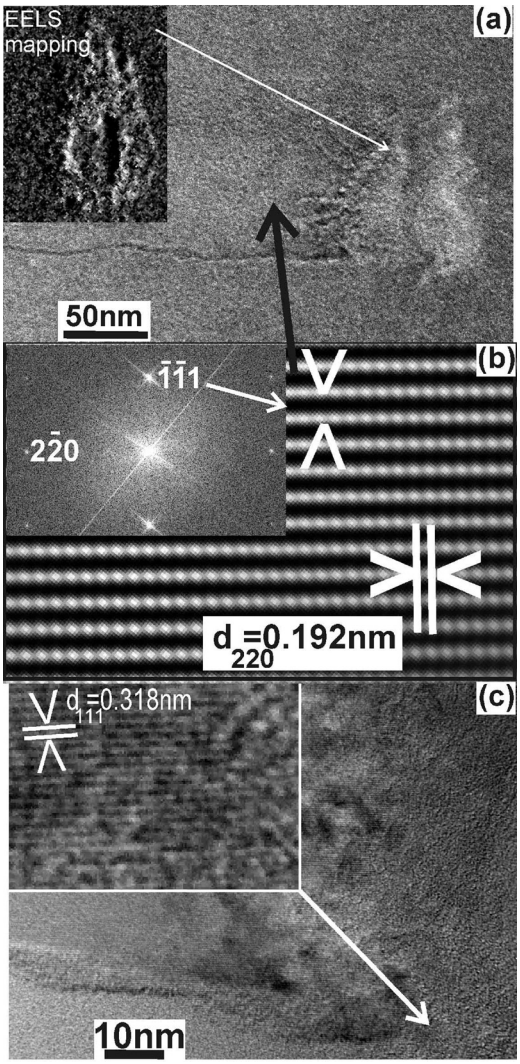

FIG. 17. (a) High magnification TEM micrograph from the head of a whisker crystallized at 413 °C for 11Ds. No misoriented sub-grains or other defects are observed. The inset is the nickel EELS mapping of the whisker, and high Ni concentration is observed only at the tip of the whisker. (b) High resolution micrograph of the whisker, the ($\bar{1}11$) and ($2\bar{2}0$) lattice planes are resolved. The inset shows the related diffraction pattern. The section of the whisker is the (110) and the direction of crystallization is the [1$\bar{1}$0]. (c) High resolution micrograph from the tip of this whisker. In the inset, the (111) lattice planes of the $NiSi_2$ precursor are resolved at high resolution. In the tip, a mixture of crystalline and amorphous material is observed.

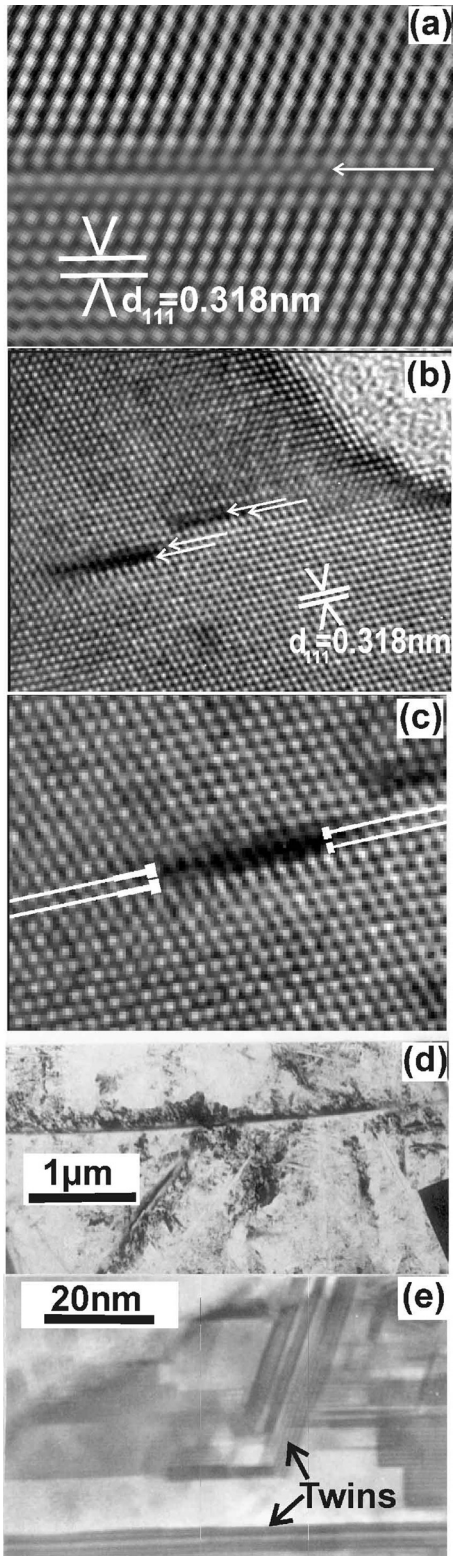

FIG. 18. Defects observed in the whiskers that are crystallized at 413 °C for 11Ds. (a) The high resolution TEM micrograph shows an extrinsic SF, such defects observed rarely in the whiskers. (b) Planar defects exhibiting very strong contrast are frequently observed. These defects resemble prismatic SFs in which two successive (111) lattice planes are missing, as shown by the two arrows. (c) The same defect at higher magnification reveals that in the reality the two lattices are severely bended in opposite directions leaving a gap in between, suggesting the formation of a plate-like precipitate there. (d) For comparison, Si that was crystallized by SPC at 600 °C, and a high density of twins is evident. (e) The same grain at high magnification, bands of twins are evident.

confirm that the tip consists of a mixture of crystalline $NiSi_2$ grains and amorphous domains.

Defects, which were found rarely in the whiskers, are extrinsic Staking Faults (SFs) as shown in the Fourier-filtered HRTEM micrograph in Fig. 18(a). Also, defects resembling extrinsic prismatic SFs, where two lattice planes are missing, exhibiting very strong diffraction contrast, are shown in Fig. 18(b). Such prismatic SFs should be very unstable; however, a more careful examination reveals that the two Si lattice planes were not missing but are highly distorted leaving a gap between them, as shown in Fig. 18(c). The gap is filled by a plate-like precipitate, probably Ni, and this defect is under further investigation. The ingrain defects of the Ni-MILC whiskers, which are crystallized at 413 °C, are compared to the ingrain defects, which are formed during the standard SPC crystallization at 600 °C, as shown in the low and high magnification TEM micrographs in Figs. 18(d) and 18(e), respectively. The grains crystallized by SPC have a high density of micro-twins of the order of 5×10^{12} cm^{-2}.[36] The crystallization by SPC is mediated by twin formation,[37] which permits a fast incorporation of the atoms at the corners of the twin planes resulting in a fast growth of the film.[38] From energetic point of view, the formation of large heavily twinned grains is more favourable than the formation of small grains free of twins, with a high density of GBs, because the formation energy of a coherent twin in silicon is 30 erg cm^{-2}, while that for GBs is 1000 erg cm^{-2}.[39,40] Therefore, SPC through twin formation is an example of the minimum action principle, where the system takes a lower energy state in the minimum time. In the pure Ni-MILC process in the range of temperatures 400 to 500 °C, the crystallization rate is very slow, giving chance to the incorporated Si atoms to find the lowest energy position in the lattice. An example of the formation by diffusion of a high quality epitaxial film at low temperature is the case of a gold film on a Si substrate. At first, a polycrystalline gold film was deposited on the 3C-SiC surface grown on the Si-substrate, then after annealing at 500 °C for 20 days, the gold was diffused through the 2.5 μm thick 3C-SiC to the SiC/Si interface forming there an almost continuous gold film.[41] This film was in perfect epitaxial relation with the Si substrate; no linear or planar defects were observed in this film in spite of the 25% misfit between Au and Si. It is worth noticing that the gold diffusivity in 3C-SiC was greatly enhanced due to the high SFs density in SiC.

IV. CONCLUSIONS

The formation of $NiSi_2$ grains under limited Ni supply condition was studied *in situ* by TEM. The nickel-disilicide grains are formed at 250 °C, and no other silicide compounds were formed in the temperature region of 250 to 400 °C. No MILC process was observed at 400 °C or below. Significant MILC was observed above 500 °C. Contamination could inhibit the formation of $NiSi_2$ as it was revealed by observations at the edge of the window, Fig. 3(f).

The structural characteristics and the growth mode of the grains crystallized by Ni-MILC, in the range of temperatures 413 to 523 °C, were systematically studied and compared to the grains grown by MILC and SPC at 600 °C. In this range of temperatures, the crystallization rate is relatively low. However, the grains exhibit some interesting characteristics, which must be attributed to the pure MILC process without involvement of SPC. The most interesting characteristics are

(I) The formation of very long whiskers with high aspect ratio.
(II) The whiskers are almost free of defects.
(III) The crystallization rate is strongly influenced by the neighbouring Ni sources, due to the long-range interaction, so the crystallization can be enhanced preferentially to a certain direction by properly distributing the Ni sources.
(IV) The whiskers are crystallized in any crystallographic direction not only along the ⟨111⟩ as it is the case for temperatures above 500 °C.
(V) The activation energy for a uniform a-c front, in the range of temperatures 400–520 °C, is approximately 2 eV, irrespectively of the size of the Ni source. In the case of the whiskers, the activation energy is reduced to 1.3 eV as it was measured by Makihira *et al.*[17] This means that the crystallization rate of the whisker is more than three times higher than the uniform a-c front.
(VI) The amount of nickel left inside the MILC crystallized region mainly depends on the annealing temperature, but not on the annealing time, and it is smaller at lower temperatures.[12] It is expected that TFTs fabricated in this range of temperatures will exhibit better performance due to the low defect density and the low Ni concentration inside the grains.

The key parameters that determine the orientation of the growing whiskers at 413 °C require further study; this problem is under investigation.

ACKNOWLEDGMENTS

This research was financially supported in the frame of a Hungarian-Greek bilateral scientific collaboration (project codes TET-10-1-2011-0570 for Hungary and HUN92 for Greece) and also by OTKA K108869. The European Union under the Seventh Framework Program under a contract for an Integrated Infrastructure Initiative, reference 312483—ESTEEM2. One of the authors J. Stoemenos would like to thank Dr. M. Miyasaka and Professor T. Asano for the useful discussions.

[1]A. Nakamura, F. Emoto, E. Fujii, A. Yamamoto, Y. Uemoto, K. Senda, and G. Kano, J. Appl. Phys. **66**, 4248 (1989).
[2]S. I. Muramatsu, Y. Minagawa, F. Oka, T. Sasaki, and Y. Yazawa, Sol. Energy Mater. Sol. Cells **74**, 275 (2002).
[3]K. C. Park, H. J. Jeon, Y. I. Kim, J. B. Choi, Y. J. Chang, Z. F. Zhan, and C. W. Kim, Solid-State Electron. **52**, 1691 (2008).
[4]M. Miyao, I. Tsunoda, T. Sadoh, and A. Kenjo, Thin Solid Films **383**, 104–106 (2001).
[5]J. H. Choi, D. Y. Kim, S. S. Kim, S. J. Park, and J. Jang, Thin Solid Films **440**, 1 (2003).
[6]M. Miyasaka and J. Stoemenos, J. Appl. Phys. **86**, 5556 (1999).
[7]F. Oki, Y. Ogawa, and Y. Fujiki, Jpn. J. Appl. Phys., Part 1 **8**, 1056 (1969).

[8]S.-W. Lee and S.-K. Joo, IEEE Electron Device Lett. **17**, 160–162 (1996).
[9]Md. Ahamad Mohiddon, M. Ghanashyam Krishna, G. Dalba, and F. Roccac, Mater. Sci. Eng., B **177**, 1108 (2012).
[10]C. Hayzelden and J. L. Batstone, J. Appl. Phys. **73**, 8279 (1993).
[11]J. Jang, S. J. Park, K. H. Kim, B. R. Cho, W. K. Kwak, and S. Y. Yoon, J. Appl. Phys. **88**, 3099 (2000).
[12]C. F. Cheng, V. M. C. Poon, W. Kok, and M. Chan, IEEE Trans. Electron Devices **50**, 1467 (2003).
[13]M. Miyasaka, K. Makihira, T. Asano, E. Polychroniadis, and J. Stoemenos, Appl. Phys. Let. **80**, 944 (2002).
[14]M. Miyasaka, K. Makihira, T. Asano, B. Pecz, and J. Stoemenos, Jpn. J. Appl. Phys., Part 1 **42**, 2592 (2003).
[15]C. Anderson and U. Kortshagen, MRS Proc. **1066**, 1066-A06-14 (2008).
[16]J. P. Colinge, IEEE Electron Devices Lett. **7**, 244 (1986).
[17]K. Makihira, H. Nozaki, T. Asano, and M. Miyasaka, "Polycrystalline semiconductors VII," in *Solid State Phenomena*, edited by T. Fuyuki, T. Sameshima, H. P. Strunk, and J. H. Werner (2003), Vol. 93, p. 207, available at http://www.scientific.net/SSP.93.207.
[18]C.-J. Su, Y.-F. Huang, H.-C. Lin, and T.-Y. Huang, Solid-State Electron. **77**, 20 (2012).
[19]Y. Ishida, G. Nakagawa, and T. Asano, J. Appl. Phys. **46**, 6437 (2007).
[20]L. A. Giannuzzi and F. A. Stevie, Micron **30**, 197 (1999).
[21]A. M. Thron, P. K. Greene, K. Liu, and K. van Benthem, Acta Mater. **60**, 2668 (2012).
[22]S. Kuwano, T. Fujita, D. Pan, K. Wang, and M. Chen, Mater. Trans. **49**, 2091 (2008).
[23]Z. Jin, G. A. Bhat, M. Yeung, H. S. Kwok, and M. Wong, J. Appl. Phys. **84**, 194 (1998).
[24]G. L. P. Berning and L. L. Levenson, Thin Solid Films **55**, 473 (1978).
[25]A. R. Joshi, T. Krishnamohan, and K. C. Saraswat, J. Appl. Phys. **93**, 175 (2003).
[26]M. Qin, M. C. Poon, L. J. Fan, M. Chan, C. Y. Yuen, and W. Y. Chan, Thin Solid Films **406**, 17 (2002).
[27]M. Wang and M. Wang, IEEE Trans. Electron Devices **48**, 1655 (2001).
[28]G. L. Olson and J. A. Roth, Mater. Sci. Rep. **3**, 1–77 (1988).
[29]R. Sinclair and T. J. Konno, J. Magn. Magn. Mater. **126**, 108 (1993).
[30]K. Holloway, R. Sinclair, and M. Nathan, J. Vac. Sci. Technol. A **7**, 1479 (1989).
[31]R. Sinclair, T. J. Konno, and D. H. Ko, in *13th International Conference on Electron Microscopy, Paris, 17–22 July* (1994), p. 429.
[32]R. Schwarz and W. Johnson, Phys. Rev. Lett. **51**, 415 (1983).
[33]R. W. Bené, J. Appl. Phys. **61**, 1826 (1987).
[34]M. Avrami, J. Chem. Phys. **9**, 177 (1941).
[35]L. Csepregi, E. F. Kennedy, and J. W. Mayer, J. Appl. Phys. **49**, 3906 (1978).
[36]L. Haji, P. Joubert, J. Stoemenos, and N. A. Economou, J. Appl. Phys. **75**, 3944 (1994).
[37]C. H. Chu, Y. M. Lu, and M. H. Hon, J. Mater. Sci. **27**, 3883 (1992).
[38]R. Drosd and J. Washburn, J. Appl. Phys. **53**, 397 (1982).
[39]H. J. Moller, J. Phys. (Paris) Colloq. **43**(C1), 33 (1982).
[40]M. Koyama, R. Yamamoto, and M. Doyama, Phys. Status Solidi **138**, 387 (1986).
[41]N. Kornilios, G. Constantinidis, M. Kayiambaki, K. Zekentes, and J. Stoemenos, Mater. Sci. Eng., B **46**, 186 (1997).